EMAS Engineering Modelling, Analysis & Simulation
THE NAFEMS JOURNAL

NAFEMS

Vol. 1, Issue 1, 2024

# Microscopic and macroscopic modeling of linear viscoelastic vibration behavior of short fiber reinforced plastics

A. Kriwet[a,1] F. Urban[a], D. Er[a], M. Stommel[b], P. Middendorf[c]

[a]Mercedes Benz AG, Mercedesstraße 102, Stuttgart 70546, Germany
[b] Institute Polymer Materials, Leibniz-Institute for Polymer Research Dresden, Hohe Straße 6, Dresden 01069, Germany
[c] Institute of Aircraft Design, University of Stuttgart, Pfaffenwaldring 31, Stuttgart 70569, Germany

## Abstract

More and more components made of short-fiber reinforced plastics are being used in modern powertrains. A reason for this is the good acoustic properties due to the lower stiffness and higher damping compared to classic metallic materials. To meet the increased customer demand regarding the acoustic sound comfort of internal combustion or electric powertrains, it is necessary to precisely predict the vibration behavior of components that are responsible for the transmission of structure-borne noise into the vehicle structure. Today's simulations often cannot satisfactorily predict the actual vibration behavior of short-fiber reinforced plastics. The required material data, in particular damping, is often obtained from static tests or considered unknown. Frequency-dependent material properties are required for a reliable prediction of the special viscoelastic properties of the short-fiber reinforced plastics. By means of a new test method based on flexural resonance vibrations, viscoelastic material data can be characterized in a frequency range between 100 Hz and 10 kHz, considering environmental conditions such as temperature and humidity. Using these material data, a simulation of the structural dynamic behavior can be performed using either of two modeling approaches: microscopic or macroscopic. The basis is the orientation of the fibers from an injection molding simulation. The microscopic modeling approach uses a two-step homogenization of the properties of the matrix, fiber and matrix-fiber-interphase followed by a spatial discretization into material databases, whilst the macroscopic modeling approach uses a one-step homogenization based on directly measured viscoelastic material data with different fiber orientation. The necessary assumptions and challenges are discussed to categorize the usage of the models in proper cases.

## Keywords

automotive, plastics, short-fiber reinforced plastics, composites, vibration, acoustics, NVH, DMA, frequency response, FEA



# 1 Introduction

The usage of short-fiber reinforced plastics (SFRP) in modern powertrains is of interest for the NVH (noise, vibration, harshness) improvement of combustion engines and electric drives. Compared to classic materials the SFRP materials stand out with their lower stiffness and higher damping. Engine and transmission brackets made of SFRP are well suited for this application and have been in series production for several years. They transmit less structure-borne noise from the drivetrain to the carbody and are therefore a crucial element in the reduction of vehicle noise. To meet increased customer

[1]Corresponding author.
E-mail address: alexander.kriwet@mercedes-benz.com (A. Kriwet)
https://doi.org/10.59972/kp48t0yu

demands regarding the acoustic comfort of modern vehicles, a precise prediction of the vibration behavior is necessary at an early stage of the development process. ([1]-[5])

The frequency range and the environmental conditions of interest depend on the application area of the SFRP structural components. Engine and transmission brackets for combustion engines show resonances at low frequencies up to 1 kHz, whereas noise problems of transmissions or electric drives typically occur at high frequencies up to 10 kHz. The temperatures close to the engine are typically up to 100 °C and the humidity varies in a wide range depending on the environment.

Today's simulations are often not able to satisfactorily predict the actual vibration behavior of SFRP in an acoustically relevant frequency range of up to 10 kHz. The required viscoelastic material properties, in particular the damping, frequently originate from a low frequency dynamic mechanical analysis (DMA) or are unknown. There is currently a lack of suitable test methods to directly determine the exact dynamic complex modulus. Its stiffness and damping have to be described in a large frequency range under consideration of ambient conditions such as temperature and humidity as well as fiber orientation. Mathematical shift approaches such as the time-temperature superposition (TTS) are used together with the DMA to extrapolate the usable frequency range but do not always provide clear and reliable results [6]. A reason for this is that TTS cannot be applied to every material [7]. Other reasons for this are a lack of reproducibility of the properties [8]. Additionally, they can only be used as relative but not as absolute values [9]. Precise material properties as well as a suitable material model are required to be able to reproduce the special viscoelastic vibration behavior of the SFRP without using an experimental model calibration or reverse engineering ([5], [10]-[12]). Isotropic modeling of composite stiffness and damping is the fundamental method for simulating the structural dynamics of SFRP. In this process, the experimentally determined storage modulus of fiber-reinforced material specimens is scaled with a factor. As a result of the uncertainty of the experimental material characterization and definition of the scaling factor, high deviations in the isotropic simulation are expected. On the other hand, the computational costs are low. As a result, isotropic calculations are still used today for early predictions of the structural dynamics. An optimization of the isotropic simulation is carried out by means of reverse engineering in comparison with experiments. [1]

Micromechanical homogenization approaches of composite stiffness represent an established method for modeling the material behavior of SFRP. For the homogenization, researchers often apply the mean-field theory. It is a mathematical-physical modeling approach in which heterogeneous stress and strain fields are described as an averaged subsection ([1], [13]-[16]). This approach originates of investigations by Eshelby [16] and leads to more advanced approaches, e.g. the Mori & Tanaka [17] or Tandon & Weng models [18]. More extended approaches such as the Double-Inclusion (DI) model by Hori et al [19] or the Reconsidered-Double-Inclusion (RDI) model by Schöneich [20] represents three-phase-homogenizations. These methods show that a more precise homogenization of the composite stiffness is achieved by considering the interphase between fiber and matrix. Methods for homogenizing the composite damping are mainly based on one-dimensional approaches. Rayleigh damping, for example, represents a mathematical method. Here, the composite damping is determined by scalar multiplication of the composite stiffness and mass matrix with scaling coefficients. Another approach is the definition of a global damping tensor, where the composite damping is equal to the damping of the matrix due to the assumption, that the main damping is contributed from the matrix material. Assuming isotropic material behavior for the matrix material, the loss factor is defined as the ratio of storage and loss modulus of the matrix ([21]-[23]). Advanced methods focus on a homogenization of the composite damping. Here, the damping tensor is defined by homogenization methods of the composite components. As already shown, the correct experimental determination of the storage and loss modulus of fiber-reinforced plastics is a challenging task. For this reason, these types of the homogenization of composite damping are reduced to simplified forms such as orthotropic isotropy. In most cases, experimental data is not used, and numerical optimizations methods of the composite damping are preferred. ([24]-[25])

The study presents a combined approach using a microscopic and a macroscopic material model enabled by a new test method to predict the actual vibration behavior of short-fiber reinforced plastics without the use of reverse engineering. As an advanced version of the flexural resonance method, the experimental approach allows to directly determine viscoelastic material properties dependent on frequency, temperature, and humidity. Two different modeling approaches were considered for this purpose, a microscopic approach based on a two-step, micromechanical homogenization, and a macroscopic approach with a one-step homogenization based on directly measured composite properties. Both approaches are compared with an isotropic and a homogenization approach according

to the Mori & Tanaka model. Furthermore, all simulation results are compared to measured structural dynamics of SFRP specimens and a component.

# 2 Methods

The fundamental basis of the holistic approach is precise viscoelastic material data characterized directly in the respective frequency, consisting of stiffness in the form of the storage modulus and damping in the form of the loss factor respectively loss modulus. An alternative approach to the established DMA is the flexural resonance method. The standard ISO 6721-3 [26] describes how material properties can be derived from resonance curves of specimens. The frequency position of the resonances and the geometry of the specimen are used to determine the storage modulus. The width of the resonance peak is used to determine the loss modulus using the 3dB method. However, it is shown that the mounting method and contactless excitation proposed in the standard only delivers good results up to frequencies of approx. 1000 Hz ([27]-[29]). More recent approaches to mounting, excitation and measurement for a much larger frequency range, by using e.g. a shaker and a laser vibrometer, can be found in ([30]-[32]). Therefore, a new experimental procedure was developed and presented in [33]. Cuboid specimens are fixed damping-free on one side to a decoupled mounting structure inside a climatic chamber and excited using a shaker. The excitation and response are measured contactless by means of a laser vibrometer. The resulting frequency response is then evaluated in the resonances for the viscoelastic material properties storage modulus and loss factor. Since not only one but multiple higher-order resonances occur in the investigated frequency range, a frequency-dependent behavior can be characterized. The schematic experimental setup and exemplary viscoelastic data are shown in Figure 1.

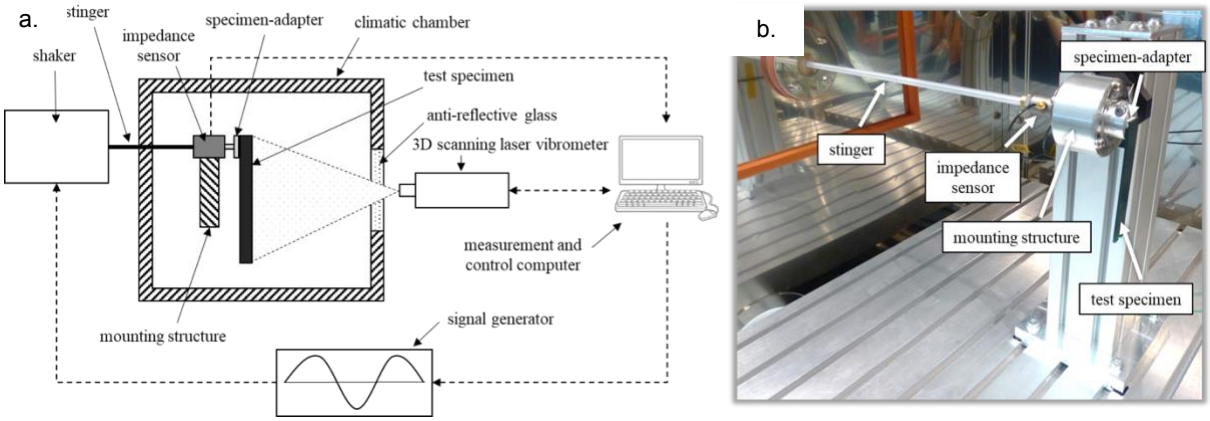


Figure 1.a. Schematic and b. real test setup [33].

For more detailed explanations of the special features and the optimization of the experimental setup to enable the generation of this data as well as a comparison with the DMA, see [33].

## 2.1 Microscopic modeling

The microscopic modeling approach uses a two-step homogenization method. First, the effective stiffness and damping tensor of the short-fiber reinforced composite is homogenized as ratio of the properties of the matrix, fiber and interphase. The homogenization is based on an advanced formulation of the Reconsidered-Double-Inclusion (RDI) model including the storage and loss modulus. Thus, the homogenization of the composite stiffness tensor is defined as

$$\boldsymbol{S}'_{RDI} = \boldsymbol{S}_S^M + \nu^F(\boldsymbol{S}_S^F - \boldsymbol{S}_S^M){:}\,\boldsymbol{B}^F + \nu^C\left(\boldsymbol{S}_S^C - \boldsymbol{S}_S^M\right){:}\,\boldsymbol{B}^C\,, \tag{1}$$

and the homogenization equation of the composite damping following as

$$\boldsymbol{S}''_{RDI} = \boldsymbol{S}_L^M + \nu^F(\boldsymbol{S}_L^F - \boldsymbol{S}_L^M){:}\,\boldsymbol{B}^F + \nu^C\left(\boldsymbol{S}_L^C - \boldsymbol{S}_L^M\right){:}\,\boldsymbol{B}^C\,, \tag{2}$$

with $\boldsymbol{S}_S^M, \boldsymbol{S}_S^F, \boldsymbol{S}_S^C$ as stiffness and $\boldsymbol{S}_L^M, \boldsymbol{S}_L^F, \boldsymbol{S}_L^C$ as damping tensor of the matrix, fiber and interphase. Furthermore, $\nu^F, \nu^C$ equals the volume fraction and $\boldsymbol{B}^F, \boldsymbol{B}^C$ equals the concentration tensor of fiber or interphase. Here, the stiffness and damping tensors of the matrix, fiber and interphase are defined as inverse of the compliance tensor with isotropic modulus, depending on whether the storage or loss modulus is fitted into the homogenization. In this context, the frequency-, temperature- and humidity-dependent storage and loss modulus of the matrix material will be used. The experimental

characterization of the viscoelastic behavior is performed by using the presented approach of the flexural vibration tests. Following this, the effective stiffness and damping tensors are combined to the complex stiffness tensor

$$\boldsymbol{S}^{*}_{RDI} = \boldsymbol{S}'_{RDI} + i\boldsymbol{S}''_{RDI}. \tag{3}$$

In the second homogenization step, material databases are generated. Here, the complex stiffness tensor is transformed into a discrete number of spatial directions $p_i$. Thereby, the construction of an ico-sphere is used [34]. Thus, a homogenous discretization of spatial transformation directions is ensured. Following this, the Maximum-Entropy-Method (MEM) is used to reconstruct the orientation distribution function (ODF) for a discrete number of second-order fiber orientation tensors $\mathbf{A}^{q}_{ii}$. The MEM uses the deviation between a given ODF in a discrete database and a calculated ODF of the fiber orientation, to minimize entropy. Accordingly, the sum function of the stiffness and damping tensors in spatial direction of the first step $\mathbf{S}^{*}_{RDI,i}$ is weighted over the spatial ODF of the second step $w^{q}_{i}$ and leads to a discrete material database with

$$\boldsymbol{S}^{*,q}_{eff,RDI} = \sum_{i}^{N} \boldsymbol{S}^{*}_{RDI,i}\, w^{q}_{i}. \tag{4}$$

The Arbitrary-Reconsidered-Double-Inclusion (ARDI) model defines this approach. Figure 2 illustrates the approach to define discrete material databases by using the ARDI model.

Following this, a filling simulation is used to predict the fiber orientation on component level. By using a process-structure coupling, the fiber orientation of the filling simulation will be transferred to the structural simulation. An assignment of the discrete material properties of the ARDI material model and the structural simulation is proceeded over the minimum error deviation between the fiber orientation of the component and the discrete ARDI database. Finally, a Prony series formulation is used to calculate the viscoelastic stiffness and damping behavior dependent on the defined conditions of frequency, temperature and humidity in a structural dynamics simulation. Detailed information about the homogenization of the composite stiffness and damping, as well as the procedure to predict the frequency response of SFRP components using the ARDI model is provided in ([35]-[36]).

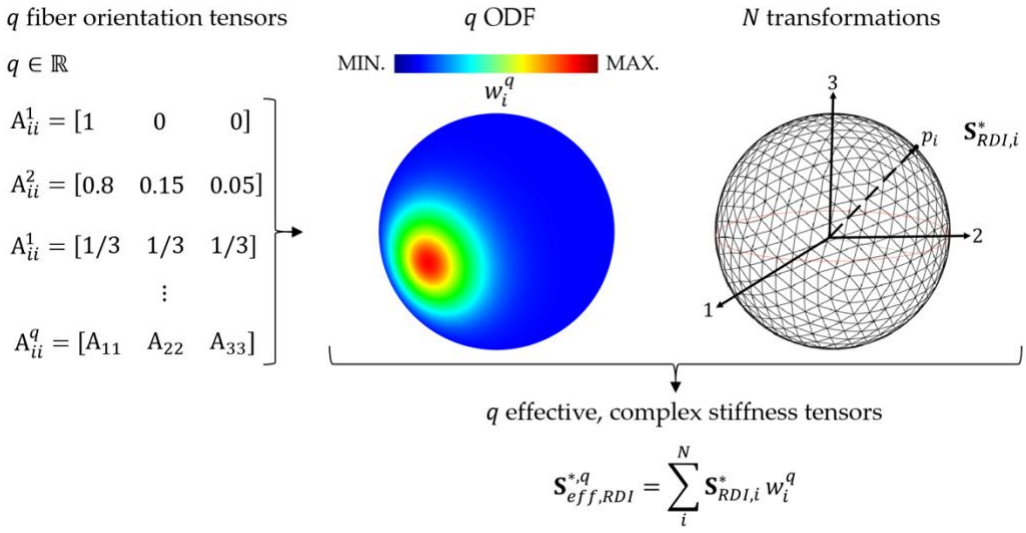


Figure 2. Method to define discrete material databases with ARDI model.

## 2.2 Macroscopic modeling

The other approach is the macroscopic modeling with single-step homogenization. It is based solely on the second-order orientation tensor and was presented in [37]. The goal is to use the viscoelastic material properties from the measurement directly and macroscopically. To assign an orthotropic stiffness matrix to each FE-element, the material data is taken directly from a large, universally valid material card using an angle-dependent description. The 2nd order orientation tensor from the injection molding simulation provides eigenvectors and eigenvalues that locally describe the main direction of the fibers and their percentage in the respective directions. Therefore, a material model linking eigenvalues and angle-dependence is required.

First, the different coordinate systems shown in Figure 3 must be explained. In the global FE-coordinate system (x,y,z) each element receives a local orientation coordinate system consisting of three eigenvectors (1,2,3) defined in the x,y,z-system. The 1-vector points in the direction in which the largest

percentage of fibers in the element is oriented. The eigenvalues ($EV_1$,$EV_2$,$EV_3$) indicate the percentage of fiber in the respective directions of the 1,2,3-system and have the sum of 1. Now a homogenization takes place by forming the resulting vector $\vec{p}_{hom}$ in the 1,2,3-system with the three eigenvalues in order to consider fiber influences of all directions in the local element. The relative deviation of the homogenized vector to the local 1,2,3-system thus contains the information about the stiffness of the element.

Figure 4 shows how to conclude an angle-dependent local element description from the deviation of $\vec{p}_{hom}$ to the 1,2,3-system. Assuming that the eigenvalue 1 is equal to 1, the other eigenvalues have to be equal to 0. In this case, the homogenized vector points in the direction of the 1-axis and all fibers in the element are oriented in this direction. Thus, the element would have an ideal relative angle of 0°-stiffness with all fibers in this direction, which corresponds to the ideal high stiffness of the 1-axis. If, on the other hand, the eigenvalues 2 or 3 are equal to 1, the homogenized vector would point in the corresponding direction. The stiffness of the local element relative to the 1-direction would thus have an ideal relative angle 90°-stiffness with all fibers in those directions, which therefore corresponds to the ideal low stiffness of the 2- and 3-axis. The real homogenized vector moves in between. By means of projection in the 12- and 13-plane, a relative deviation angle $\phi$ and $\theta$ from the 1-axis is obtained, which varies between 0° and 90°.

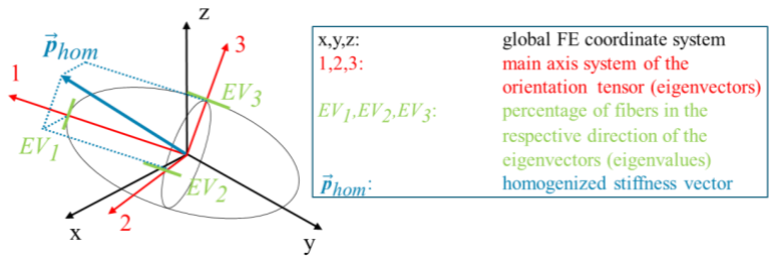


Figure 3. Coordinate systems of a local macroscopic FE-element [37].

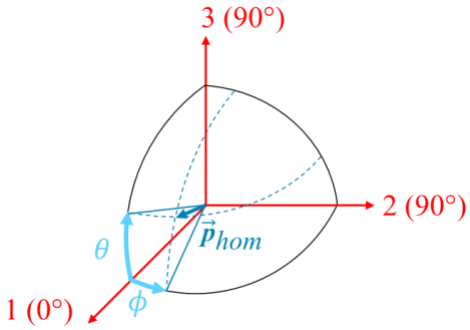


Figure 4. Local orientation projection into the 12- and 13-plane [37].

Therefore, the local stiffness in the 1,2,3-coordinate system in the 1-direction results from the relative deviation of $\phi$ and $\theta$ from the 1-axis with the storage modulus $E'(\phi)$ and $E'(\theta)$ taken from the angle-dependent material card to

$$E_1' = \frac{E'(\phi)\cdot EV_2 + E'(\theta)\cdot EV_3}{EV_2 + EV_3}. \quad (5)$$

The eigenvalues are used to allow a relative weighting of the fiber quantity for the respective direction. To calculate the stiffness in the 2- and 3-directions, the quadrants have to be switched and the homogenized vector has to be completed to a Cartesian coordinate system. Its projected angular deviation from the 2-axis and to the 3-axis results in the respective stiffness

$$E_2' = \frac{E'(90°-\phi)\cdot EV_1 + E'(90°)\cdot EV_3}{EV_1 + EV_3}. \quad (6)$$

$$E_3' = \frac{E'(90°)\cdot EV_2 + E'(90°-\theta)\cdot EV_1}{EV_2 + EV_1}. \quad (7)$$

Equations (5-7) can be used in the same way for the loss modulus. Thus, the complex orthotropic stiffness matrix can now be filled locally for the considered element:

$$\begin{bmatrix}\sigma_{11}\\ \sigma_{22}\\ \sigma_{33}\\ \sigma_{12}\\ \sigma_{13}\\ \sigma_{23}\end{bmatrix} = \begin{pmatrix} \frac{1-\nu_{23}\nu_{32}}{D}E_1^* & \frac{\nu_{13}\nu_{32}+\nu_{12}}{D}E_2^* & \frac{\nu_{12}\nu_{23}+\nu_{13}}{D}E_3^* & 0 & 0 & 0 \\ & \frac{1-\nu_{13}\nu_{31}}{D}E_2^* & \frac{\nu_{21}\nu_{13}+\nu_{23}}{D}E_3^* & 0 & 0 & 0 \\ & & \frac{1-\nu_{12}\nu_{21}}{D}E_3^* & 0 & 0 & 0 \\ & & & G_{12}^* & 0 & 0 \\ & sym & & & G_{13}^* & 0 \\ & & & & & G_{23}^* \end{pmatrix} \begin{bmatrix}\varepsilon_{11}\\ \varepsilon_{22}\\ \varepsilon_{33}\\ 2\varepsilon_{12}\\ 2\varepsilon_{13}\\ 2\varepsilon_{23}\end{bmatrix}, \quad (8)$$

where

$$D = 1 - \nu_{12}\nu_{21} - \nu_{13}\nu_{31} - \nu_{23}\nu_{32} - 2\nu_{21}\nu_{32}\nu_{13}, \quad (9)$$

and

$$\nu_{kj} = \frac{E_k^*}{E_j^*}\nu_{jk}; j,k := \{1,2,3\}. \quad (10)$$

The shear modulus in Equation (8) can be approximated in the form of:

$$G_{jk}^* = \frac{E_j^* E_k^*}{E_j^* + 2\nu_{jk}E_j^* + E_k^*}; j,k := \{1,2,3\}, \quad (11)$$

described in detail in [38]. Finally, it must be transformed back into the global x, y, z-coordinate system with the coordinates of the eigenvectors in order to perform the FE-calculation.

In order to be able to fill equations (5-7) with angle-dependent storage and loss modulus, a comprehensive material card is required. Therefore, cuboid specimens are cut out of a flat injection molded plate in different orientations relative to the flow direction, see Figure 5.

However, the cutting direction has nothing to do with the fiber orientation angles required in the material model. To conclude from a cutting orientation to a fiber orientation, the real fiber composition of the specimens must be determined. The measured specimens have an averaged stiffness of all fiber orientation distributions that occur in them. It is assumed that the averaged deviation of all macroscopic elements of a specimen corresponds to the viscoelastic properties measured with it. To determine the correct averaged orientation angle, the material model must now be calculated backwards. To do this, the averaged absolute orientation direction in the global coordinate system is determined for each cut-out specimen using the injection molding simulation of the plate from which the specimens are taken. These directions are shown as arrows in Figure 6 and differ slightly from each other. The angular deviation from their respective cutting orientation yields the averaged fiber orientation angle. It directly corresponds to the measured viscoelastic properties of the specimen. This is shown as an example in Figure 6 for the 45°-specimen. The determined averaged angles can now be used for inter- and extrapolation of the material card in the angular domain and thus in the FE-calculation.

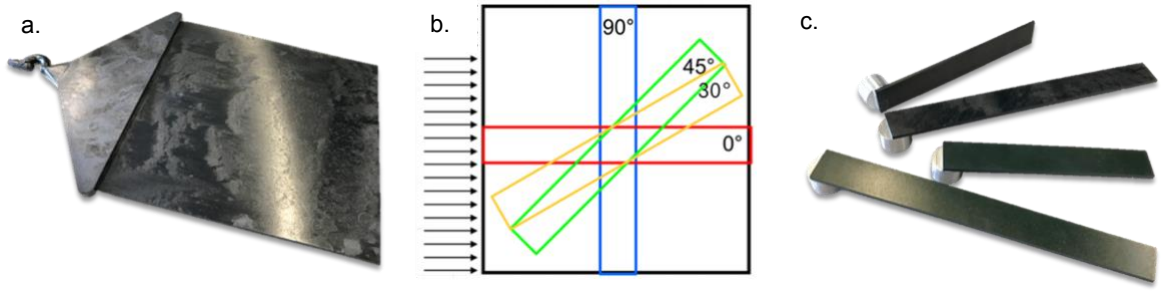


Figure 5. Preparation of test specimens (a. injection molded plate, b. cutting orientations, c. test specimens with specimen-adapter) [37].

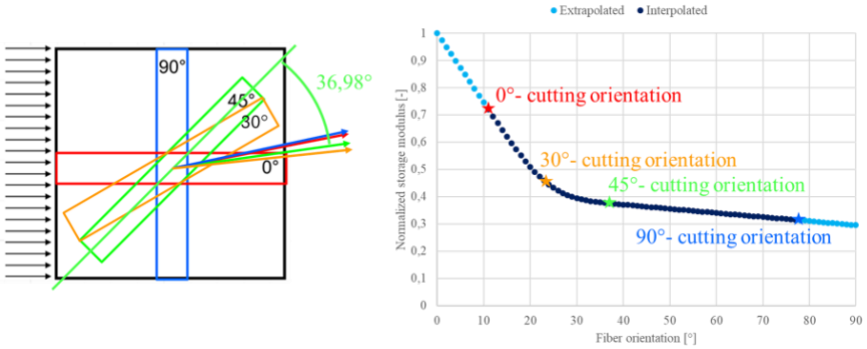


Figure 6. Conclusion from a cutting orientation to an averaged fiber orientation [37].

# 3 Results and Discussion

For the investigations, polyamide 6.6 with 50 weight percent short glass fibers (PA66-GF50) is used. Within the scope of the comparison, on the one hand cuboid test specimens taken from injection molded specimen plates in different orientations to the direction of injection molding are used. On the other hand, a structural component of a powertrain is examined: a transmission bracket. Standard environmental condition is considered for both comparisons: Room temperature (23°C) and completely dry air at 0% relative humidity.

## 3.1 Input data

The necessary input data are limited to the injection molding process simulation of the specimen plate and the transmission bracket as well as the viscoelastic material data from the measurements. The injection molding process simulation is carried out with the software CADMOULD. Specimens at representative positions distributed over the specimen plate in the injection molding simulation are evaluated in comparison to micro-CT analysis of the real fiber orientation distribution. Thereby, the process simulation is optimized with respect to the fiber orientation. Subsequently, the calibrated injection molding model is used for both the specimen plate and the component. The characterization of the viscoelastic properties is carried out within a climatic chamber analogous to the experimental procedure in Figure 1. For the microscopic approach, specimens of the pure matrix material are examined. For the macroscopic approach, short fiber reinforced specimens are characterized at a total of four different angles to the injection molding direction of the specimen plate.

## 3.2 Specimen

The material models are compared by examining the specimen resonances through the whole frequency range. The stiffness is represented by the frequency position and the damping by the amplitude of the peak. The investigated specimens have a dimension of 140x15x2 mm, with 5 mm at one end representing the mounting and excitation area with a fixed-free boundary condition. The characterization of the dynamic behavior is conducted according to Figure 1 within a climatic chamber at constant environmental conditions. Excitation is performed by means of a shaker/stinger combination with direct measurement of the excitation force. The acceleration response is measured on the surface of the specimen. By normalizing the response with the excitation, a comparison by means of a frequency response function (FRF) between measurement and simulation is possible.

The finite element (FE) model is built analogously to the experiment, see Figure 7. The specimen is meshed with C3D20-elements. To couple the full fiber orientation data of the injection molding simulation with the FE-model, ten layers within the thickness of the specimen are modelled with an element aspect ratio of 12,5. In total it takes 3360 elements and 16453 nodes for the specimen. 5 rows of nodes at one end, 53 nodes in total, define the boundary and excitation area. Subsequently the fiber orientation from the injection molding simulation is mapped onto the FE-Mesh by using the nearest neighbor method within the software CONVERSE 4.4.0.2. Each element receives a second-order orientation tensor for use in the microscopic and macroscopic model.

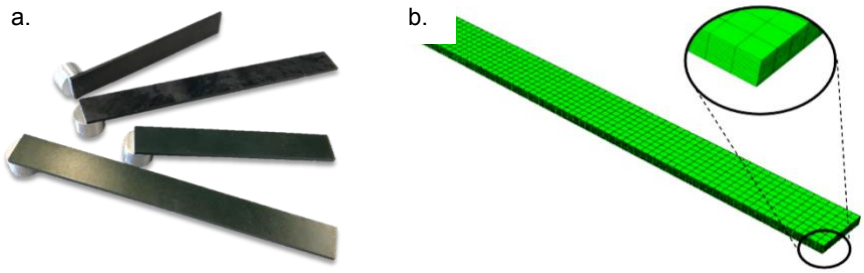


Figure 7. Cuboid specimen, a. Specimen with characterization adapter, b. CAE-Model [37].

The FE-simulation takes place in the FE-solver ABAQUS using the UMAT-interface for the material models and a Direct-solution steady-state dynamic analysis in the respective frequency steps. Figure 8 presents the results of the comparison between the measured and the simulated FRF of the microscopic and macroscopic approach are shown for four different specimen orientations (displayed in Figure 5).

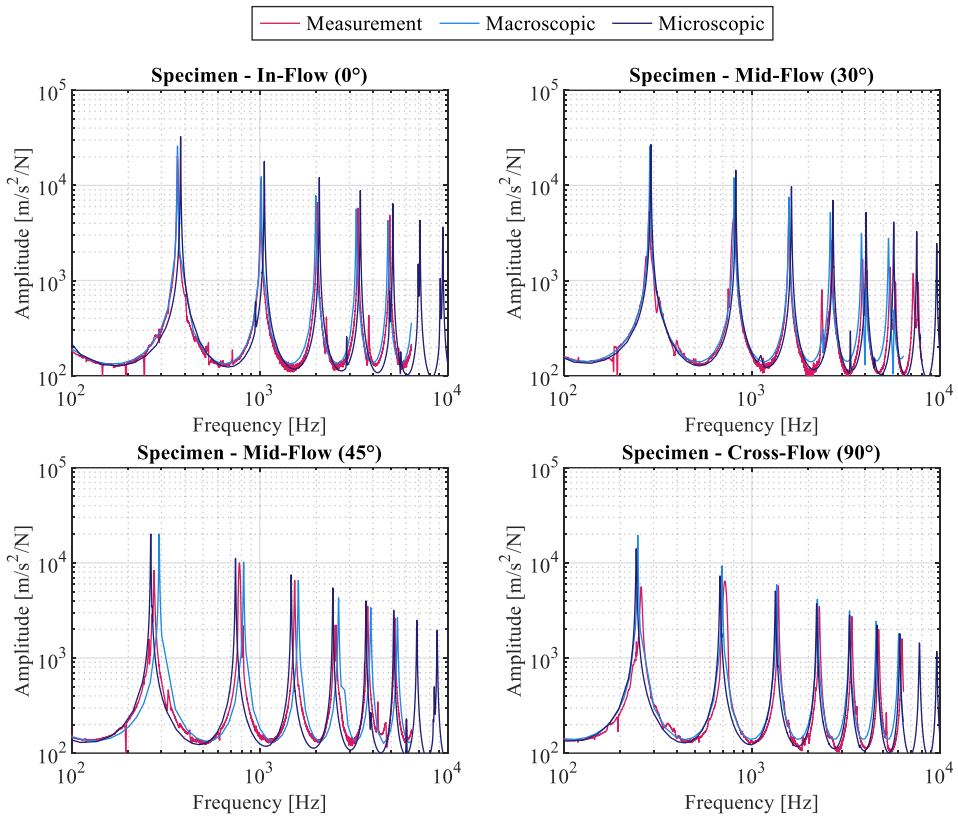


Figure 8. Comparison of the macroscopic and the microscopic approach with measurements of different oriented cuboid specimens at 23°C and 0% humidity.

On a global frequency scale, a good accuracy of both modeling techniques can be observed in comparison to the measurement. To point out the differences between the two methods, a closer evaluation of the resonance peaks is required. Therefore, the 5th and 6th superior resonances were investigated for each specimen orientation in more detail. Figure 9 shows the relative deviations of the microscopic and macroscopic model are similar for all specimen orientations. However, the global resonances of the microscopic model for the 0° and 30° specimen are at higher frequencies in comparison to the measurement, due to an increased stiffness. For the 45° and 90° specimen, the resonances are at lower frequencies, due to a decreased stiffness. The macroscopic approach instead shows lower resonance frequencies and therefore a lower stiffness prediction in all cases, except for the 45° orientation, where it is higher than the measurement. However, significant differences can be observed at the inferior resonances of the measurement in comparison to both simulations. An example for this is the small resonance peak of the microscopic model just below 5000 Hz for the 0° specimen or the resonance at 3300 Hz for the 45° specimen. These resonances cannot be observed in the measurement. This can be explained by the homogenization approach of the microscopic model. Here, an increased deviation of the local numerical fiber orientation of the process simulation occurs. This leads to an insufficient homogenization of the local stiffness. The macroscopic approach shows an improved prediction of the inferior resonances. The resonance at 2400 Hz and the twin-peak at 4000 Hz of the 30° specimen are good examples.

For the prediction of the superior resonance amplitudes, the micro- and macroscopic modeling approach only show minor differences. The microscopic model predicts consistently higher amplitudes. This is due to the homogenization approach. The damping of the matrix, fiber and matrix-fiber-interphase are considered by the ARDI model, but further damping influences like composite inhomogeneities are not taken into account. The macroscopic approach, however, is better at predicting composite damping. This is due to the one-step homogenization with the directly measured values of the composite material.

Figure 10 shows the FRF of the micro- and macroscopic model in comparison to an isotropic as well as a Full-Mori-Tanaka (FMT) modeling approach.

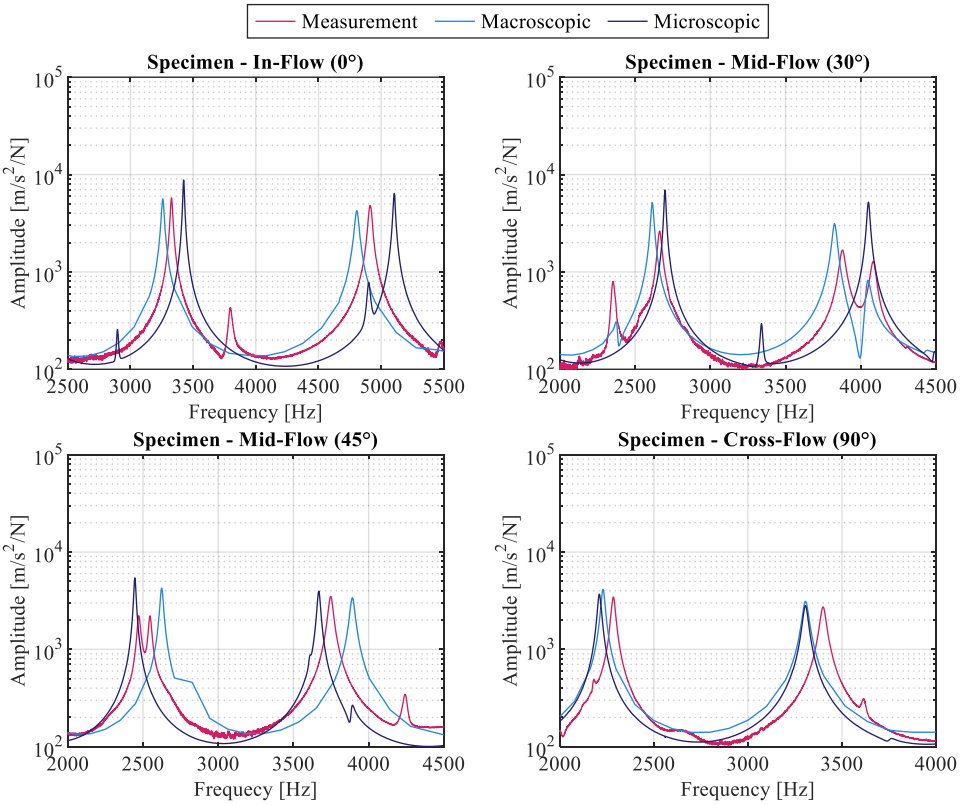


Figure 9. Zoom into the frequency range of the cuboid specimens, as an example the 5th and 6th resonance order are shown for each orientation.

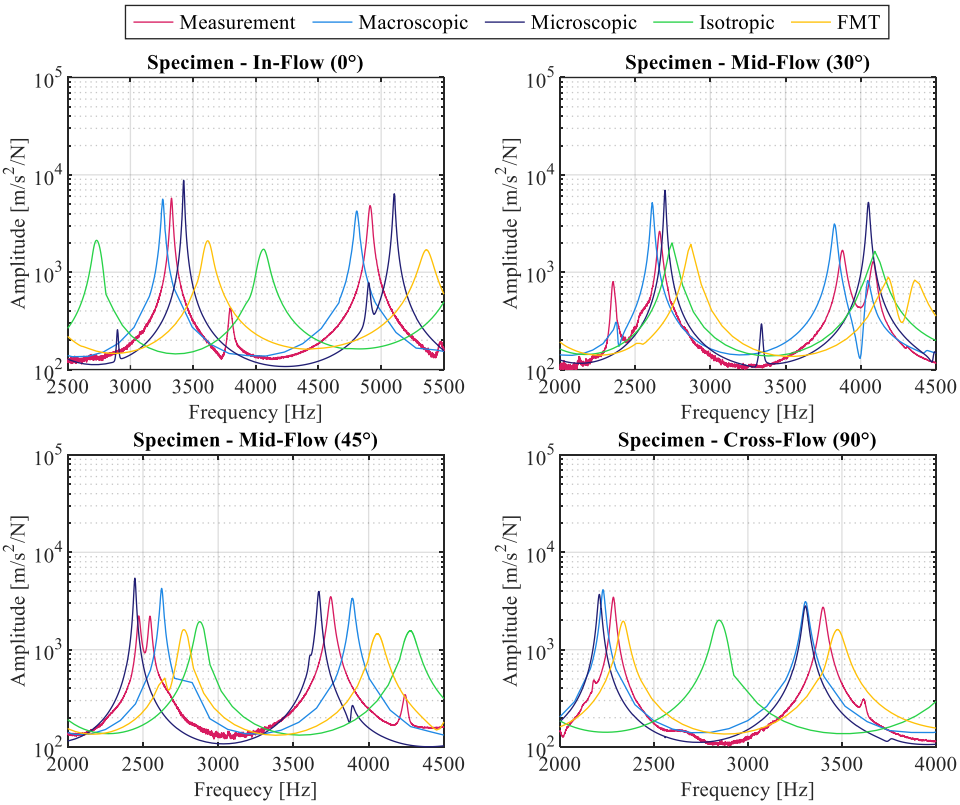


Figure 10. Zoom into the frequency range of the cuboid specimens, as an example the 5th and 6th resonance order are shown for each orientation.

For the isotropic model, the data sheet value of the tensile modulus is multiplied by a scaling factor of 0,65 [1] and defined as a global stiffness value independent of direction. The FMT model is a two-step homogenization approach. A Mori & Tanaka modeling of the stiffness defines the first step and a reconstruction of discrete spatial material databases through the MEM defines the second step. As a common value, 1% modal damping is defined as material damping in both cases.

The FRFs of the isotropic approach are identical in all orientation cases and are therefore not suited for predicting the structural dynamic behavior. The FMT approach shows an improved prediction of the FRFs with respect to the different orientations of the specimens. However, the predicted stiffness is higher in all orientation cases as well as in comparison to the micro- or macroscopic approach. This can be explained by a lack of calibration of the material properties, since only the tensile stiffness of the material data sheet is used. Furthermore, the damping at given temperature and humidity is overestimated with the defined value of 1% modal damping. The resonance peaks are lower compared to the measurement or the micro- or macroscopic approaches. Missing orientation dependence of the damping also becomes apparent when comparing 0° and 90° specimens. The methods and values used for stiffness and damping represent the quality of material data usually available in the industry.

## 3.3 Component

The transmission bracket in the left side of Figure 11 is a representative example for the application of the material models on component level. It is a thin-walled structure that exhibits both superior (global) and inferior (local) structural dynamic modes. The dimensions of the transmission bracket are approx. 228x82x121 mm with a weight of 254 g. The structural dynamics are characterized inside a climatic chamber at constant ambient conditions. It is suspended in a freely supported state with temperature-resistant aramid ropes at two points. Furthermore, it is excited by means of a shaker/stinger combination to determine the FRF, analogously to the procedure for the specimens.

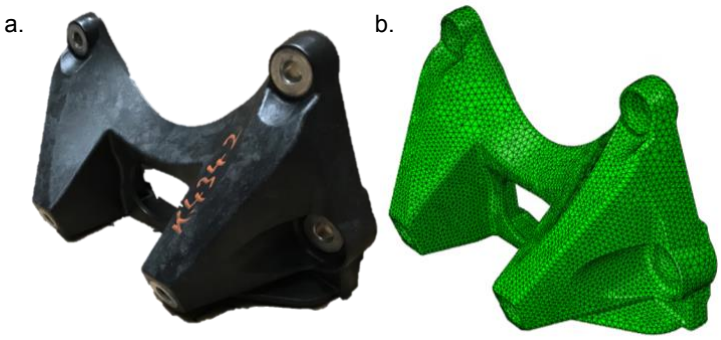


Figure 11.a. Transmission bracket, component, b. CAE-Model.

The transmission bracket is modeled using C3D8 elements. To optimize the computational effort, only four elements across the overall wall thickness were defined for meshing. This leads to a reduction of the mapped fiber orientation data from the process simulation. However, the effect on the results is small at component level compared to the specimens. Thus, a total of 79635 elements and 137162 nodes were used to model the transmission bracket, as shown in Figure 11.b. The structural dynamics simulation is performed with a direct-solution steady-state dynamic analysis using the UMAT interface of the ABAQUS 2017 solver. The measured FRF compared to the FRF of the micro- and macroscopic model is shown in Figure 12.

The prediction quality of the resonance frequencies and therefore the stiffness by the micro- and macroscopic model are similar. The largest relative deviation in comparison to the measurement is seen at the superior resonance at 300 Hz. Comparable to the investigations on specimen level, the macroscopic model allows an improved prediction of the minor resonances on component level. As an example, the resonance peaks at 2200 Hz and 3700 Hz can be identified. However, a comparison of the damping is difficult, since the measurement shows high damping in the lower frequency range. This is caused by the experimental suspension, which influences the superior, global resonances of the bracket. In the frequency range of inferior, local resonances above 2000 Hz, a comparison of the amplitudes is however possible. In general, both approaches allow a good prediction of the overall amplitude. Similar to the results of the specimens, the damping of the microscopic model is lower compared to the macroscopic model. Larger deviations in comparison with the measurement can be attributed to excessive damping due to the suspension.

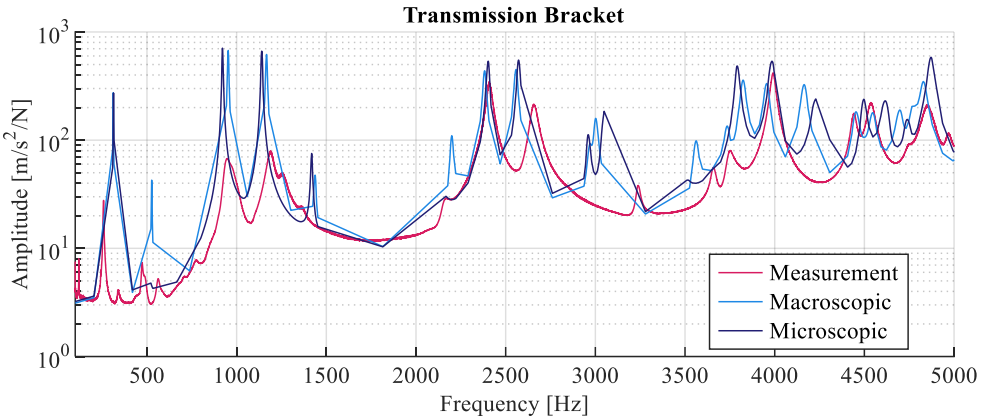


Figure 12. Comparison of the macroscopic and the microscopic approach with measurements of the transmission bracket at 23°C and 0% humidity.

Figure 13 shows the FRF results of the simulations with isotropic and FMT model in the frequency range of inferior resonances. The composite stiffness is defined with the same approach as on specimen level. Furthermore, the modal damping is set to a value of 0.3% by iterative optimization for a better comparison with the measurement.

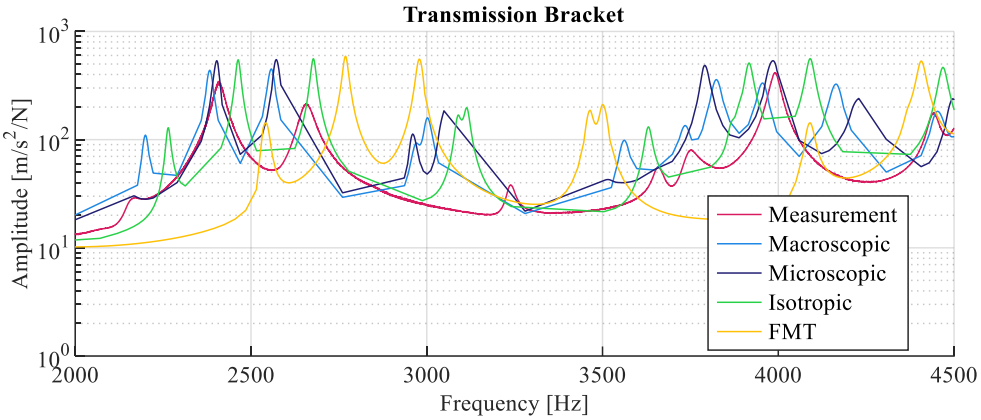


Figure 13. Zoom into the frequency range of the transmission bracket and comparison with state-of-the-art modeling using 0,3% modal damping.

The isotropic approach predicts the composite stiffness and thus the resonance positions of the measured FRF with a higher accuracy compared to the FMT approach. The FMT again shows an increased composite stiffness by a shift of the resonances to higher frequencies. However, in comparison, it is apparent that the stiffness prediction deviates many times more than by the micro- or macroscopic approach. A prediction of the damping by the isotropic or FMT approach is still only possible with an accurate comparison with an experiment.

# 4 Conclusions

In this study, an advanced approach for characterizing and modeling the viscoelastic material behavior of short-fiber reinforced plastics for an accurate prediction of the structural dynamics behavior was presented. Therefore, a method for experimental flexural resonance characterization was presented. Thereby, a characterization of the viscoelastic material data of pure plastic matrix and fiber reinforced material in a wide frequency range is possible. Two advanced material modeling methods for homogenization of the composite stiffness and especially damping were presented: a two-step microscopic and a one-step macroscopic approach. These were compared with an isotropic approach as well as a micromechanical modeling by means of a Full Mori & Tanaka (FMT) model. In both cases, tensile modulus of material data sheets was used for the homogenization of the composite stiffness. Furthermore, modal damping was applied. To assess the prediction accuracy of the models, differently oriented specimens as well as a composite transmission bracket of a powertrain were investigated. The

structural dynamic behavior was compared by means of force-normalized frequency response functions of measurement and simulation.

It was shown on specimen and component level, that the macroscopic approach provides a sufficient prediction of the resonance peaks of the superior and inferior structural dynamics. However, the effort required to determine the necessary material behavior is increased compared to the microscopic approach. Both show a similar prediction accuracy of stiffness and damping compared with the measurements. To achieve such a high prediction quality of the structural dynamics, both a high accuracy of the fiber orientation by the process simulation as well as a reliable experimental characterization of the frequency-dependent viscoelastic material behavior at defined ambient conditions is necessary. In comparison, neither the isotropic nor the FMT allows a comparable prediction accuracy of the structural dynamics. In particular, the damping cannot be estimated without an iterative optimization.

It can be concluded, that for an initial estimation of the structural dynamics in an early development phase, the isotropic or FMT approach is sufficient. In an advanced development phase, in which the composite material is under development and an injection molding model based on a given geometry is available, the microscopic approach allows an improved prediction accuracy. In a late development phase, in which the composite material has already been determined, the macroscopic approach allows the highest prediction accuracy.

# 5 References


[1] M. Stommel, M. Stojek and W. Korte, FEM zur Berechnung von Kunststoff- und Elastomerbauteilen. Carl Hanser Verlag GmbH Co KG, 2018.

[2] H. Kremer, „Materialdatenermittlung thermoplastischer Kunststoffe für Körperschallsimulationen auf Basis von Reverse Engineering“, PhD Thesis, 2014.

[3] K. Raschke and W. Korte, „Faserverstärkte Motorbauteile besser berechnen“, Kunststoffe, vol. 109, pp. 184-189, 2019.

[4] W. Michaeli, C. Hopmann and H. Kremer, „Materialdatenermittlung für Akustiksimulationen mittels Reverse Engineering: Akustisches Verhalten von Kunststoffen“, Kunststoffe, vol. 102, pp. 5-7, 2012.

[5] M. op de Laak and M. Hauth, “Noch schneller zur Zylinderkopfhaube”, Kunststoffe, vol. 94, pp. 126-130, 2004.

[6] K. P. Menard, Dynamic Mechanical Analysis. Boca Raton: Crc Press, 2020.

[7] E. T. J. Klompen and L. E. Govaert, Mechanics of Time-Dependent Materials, vol. 3, no. 1, pp. 49–69, 1999, doi: https://doi.org/10.1023/a:1009853024441.

[8] B. Wampfler, S. Affolter, A. Ritter and M. Schmid, Messunsicherheit in der Kunststoffanalytik. Carl Hanser Verlag GmbH Co KG, 2017.

[9] Standard Test Method for Plastics: Dynamic Mechanical Properties: In Flexure (Three-Point Bending). ASTM D5023-15, 2016, doi: https://doi.org/10.1520/D5023-15.

[10] M. Giersbeck, K. Hornberger and A. Kech, „Virtuelle Bauteilentwicklung“, Kunststoffe, vol. 101, pp. 50-53, 2011.

[11] C. Hopmann, W. Michaeli and H. Kremer, „Frequenzabhängiges Verhalten von Kunststoffen“, Kunststoffe, vol. 102, pp. 64-66, 2012.

[12] S. Pischinger, W. Michaeli, M. Joerres, C. Steffens, M. Atzler and T. Arping, “Verfahren zur akustischen Simulation von Kunststoffbauteilen”, MTZ - Motortechnische Zeitschrift, vol. 70, no. 9, pp. 692–701, Sep. 2009, doi: https://doi.org/10.1007/bf03225522.

[13] H. J. Böhm, A short introduction into basic aspects of continuum micromechanics. Institute of Lightweight Design and Structural Biomechanics (ILSB), 2008.

[14] O. Pierard, “Micromechanics of inclusion-reinforced composites in elasto-plasticity and elasto-viscoplasticity modeling and computation”, PhD Thesis, Katholische Universität Löwen, 2006.

[15] R. Hill, “Elastic properties of reinforced solids: Some theoretical principles”, Journal of the Mechanics and Physics of Solids, vol. 11, no. 5, pp. 357–372, Sep. 1963, doi: https://doi.org/10.1016/0022-5096(63)90036-x.

[16] “The determination of the elastic field of an ellipsoidal inclusion, and related problems”, Proceedings of the Royal Society of London. Series A. Mathematical and Physical Sciences, vol. 241, no. 1226, pp. 376–396, Aug. 1957, doi: https://doi.org/10.1098/rspa.1957.0133.

[17] T. Mori and K. Tanaka, “Average stress in matrix and average elastic energy of materials with misfitting inclusions,” Acta Metallurgica, vol. 21, no. 5, pp. 571–574, May 1973, doi: https://doi.org/10.1016/0001-6160(73)90064-3.

[18] G. P. Tandon and G. J. Weng, “The effect of aspect ratio of inclusions on the elastic properties of unidirectionally aligned composites”, Polymer Composites, vol. 5, no. 4, pp. 327–333, Oct. 1984, doi: https://doi.org/10.1002/pc.750050413.

[19] M. Hori and S. Nemat-Nasser, “Double-inclusion model and overall moduli of multi-phase composites”, Mechanics of Materials, vol. 14, no. 3, pp. 189–206, Jan. 1993, doi: https://doi.org/10.1016/0167-6636(93)90066-z.

[20] M. Schöneich, „Charakterisierung und Modellierung viskoelastischer Eigenschaften von kurzglasfaserverstärkten Thermoplasten mit Faser-Matrix Interphase“, PhD Thesis. Universität des Saarlandes, 2016, doi: http://dx.doi.org/10.22028/D291-23208

[21] M. Bienert, “Warum der ganze Aufwand? Eine Einführung in die experimentelle Modalanalyse”, in Polytec Anwenderkonferenz, 2022.

[22] M. Möser, Ed., Messtechnik der Akustik. Berlin, Heidelberg: Springer Berlin Heidelberg, 2010. doi: https://doi.org/10.1007/978-3-540-68087-1.

[23] K. Magnus, K. Popp and W. Sextro, Schwingungen. Wiesbaden: Springer Fachmedien Wiesbaden, 2016. doi: https://doi.org/10.1007/978-3-658-13821-9.

[24] P. Kumar, R. Chandra, and S. P. Singh, “Interphase Effect on Fiber-Reinforced Polymer Composites”, Composite Interfaces, vol. 17, no. 1, pp. 15–35, Jan. 2010, doi: https://doi.org/10.1163/092764409x12580201111502

[25] A. Treviso, B. Van Genechten, D. Mundo and M. Tournour, “Damping in composite materials: Properties and models”, Composites Part B: Engineering, vol. 78, pp. 144–152, Sep. 2015, doi: https://doi.org/10.1016/j.compositesb.2015.03.081.

[26] Plastics — Determination of dynamic mechanical properties — Part 3: Flexural vibration — Resonance-curve method. ISO 6721-3, 2021.

[27] J.-M. Berthelot, M. Assarar, Y. Sefrani and A. E. Mahi, “Damping analysis of composite materials and structures”, Composite Structures, vol. 85, no. 3, pp. 189–204, Oct. 2008, doi: https://doi.org/10.1016/j.compstruct.2007.10.024.

[28] P. Bonfiglio and F. Pompoli, “Determination of the dynamic complex modulus of viscoelastic materials using a time domain approach”, Polymer Testing, vol. 48, pp. 89–96, Dec. 2015, doi: https://doi.org/10.1016/j.polymertesting.2015.09.016.

[29] R. M. Crane and J. W. Gillespie, “Characterization of the vibration damping loss factor of glass and graphite fiber composites”, Composites Science and Technology, vol. 40, no. 4, pp. 355–375, Jan. 1991, doi: https://doi.org/10.1016/0266-3538(91)90030-s.

[30] J. Ilg, S. J. Rupitsch and R. Lerch, “Determination of frequency and temperature dependent mechanical material properties by means of an Inverse Method”, WIT Transactions on Engineering Sciences, Jun. 2013, doi: https://doi.org/10.2495/mc130091.

[31] K. De Belder, R. Pintelon, C. Demol and P. Roose, “Estimation of the equivalent complex modulus of laminated glass beams and its application to sound transmission loss prediction”, Mechanical Systems and Signal Processing, vol. 24, no. 3, pp. 809–822, Apr. 2010, doi: https://doi.org/10.1016/j.ymssp.2009.11.001.

[32] F. Cortés and M. J. Elejabarrieta, “Viscoelastic materials characterisation using the seismic response”, Materials & Design, vol. 28, no. 7, pp. 2054–2062, Jan. 2007, doi: https://doi.org/10.1016/j.matdes.2006.05.032.

[33] F. Urban, B. Armbruster and P. Middendorf, “Development and validation of a method for linear-viscoelastic characterization of the dynamic complex modulus of short-fiber reinforced plastics using flexural resonances”, Polymer Testing, vol. 94, p. 107055, Feb. 2021, doi: https://doi.org/10.1016/j.polymertesting.2021.107055.

[34] K. Breuer, M. Stommel, and W. Korte, “Analysis and Evaluation of Fiber Orientation Reconstruction Methods,” Journal of Composites Science, vol. 3, no. 3, p. 67, Jul. 2019, doi: https://doi.org/10.3390/jcs3030067.

[35] A. Kriwet and M. Stommel, “Arbitrary-Reconsidered-Double-Inclusion (ARDI) Model to Describe the Anisotropic, Viscoelastic Stiffness and Damping of Short Fiber-Reinforced Thermoplastics”, Journal of Composites Science, vol. 4, no. 2, p. 37, Apr. 2020, doi: https://doi.org/10.3390/jcs4020037.

[36] A. Kriwet and M. Stommel, “The Impact of Fiber Orientation on Structural Dynamics of Short-Fiber Reinforced, Thermoplastic Components—A Comparison of Simulative and Experimental Investigations”, Journal of Composites Science, vol. 6, no. 4, p. 106, Apr. 2022, doi: https://doi.org/10.3390/jcs6040106.

[37] F. Urban and P. Middendorf, “Macroscopic Modeling of the Linear Viscoelastic Vibration Behavior of Short Fiber Reinforced Plastics,” SAMPE 2020 | Virtual Series, 2020, doi: https://doi.org/10.33599/382/s.20.0015.

[38] P. Kohnke, ANSYS - engineering analysis system theoretical manual for Rev. 4.4, 5th ed. Houston: Swanson Analysis Systems Inc., 1989.